Notes on the SHMS optics in the 2017-18 run period

Holly Szumila-Vance*

Jefferson Lab
hszumila@jlab.org

Abstract

This note illustrates some of the procedures used in the commissioning of the Super High Momentum Spectrometer (SHMS) optics in the 12 GeV era. All SHMS magnets were studied prior to the beam running with probes installed to measure the central fields and were characterized such that the magnets are set by current to obtain the desired field during beam running conditions. The modifications to the field setting program is discussed. Additionally, the matrix optimization algorithm and results are discussed.

1 Introduction

The SHMS is the newly installed spectrometer in Hall C for the upgraded 12 GeV electron beam physics program at Jefferson Lab. The detector hut includes all new and upgraded detectors for the higher momentum physics. The SHMS has an acceptance of 4 mSr and momentum resolution of 0.05% ($\delta P/P$). It can be set to a central momentum in the range of 1–11 GeV/c and can rotated to measure particles at scattering angles of 5.5–40 degrees from the beam line. The dipole has an 18.4 degree vertical bend. The SHMS spectrometer was first turned on during the spring of 2017 and was rigorously commissioned with beam and experiments beginning in the winter of 2017.

The SHMS beam line after the target first includes the horizontal bender (HB) magnet which steers particles in the horizontal plane away from the the incident beam line. Particles then pass through the three quadrupole magnets (Q1, Q2, Q3) that focus the beam into the spectrometer dipole. Q1 and Q3 mostly focus the beam in the vertical plane and Q2 focuses the beam in the horizontal plane. All of the magnets in the SHMS are set by current. The spectrometer dipole has a probe installed during beam running, but it is located in the exit fringe field and shows significant drop off when compared to measurements of the central field values. As such, extensive studies in the summer of 2017 installed probes in the center of the magnets to study the central field behavior as a function of current. The data from these studies is stored in a repository at [4].

The commissioning of the SHMS used carbon elastic scattering and the 4.4 MeV carbon excited peak for tuning the quadrupole strengths relative to the spectrometer dipole and HB magnets. Two carbon sieves are used with one having the center hole located at the center of the sieve whereas the other shifted sieve has the same sieve pattern, but all holes are offset horizontally by half the distance between the holes. The sieve made it possible to tune the quads by looking at the focal plane distributions of the 4.4 MeV carbon excited peak, and the sieve was later used with multi-foil extended carbon targets to record data for the optimization of the reconstruction matrix elements. Both carbon and hydrogen data were useful for understanding the pointing and angle offsets and the offsets of the central momentum for various settings.

*

The focus of this document is to record the central field measurement studies of the SHMS magnets, to document the methodology for setting the magnets, and to record the initial tuning, performance, and matrix optimization of the reconstruction matrix elements.

2 SHMS field measurements

The SHMS magnets were tested between 2015–2017 with most of the central field studies taking place at the end of the summer 2017. Lakeshore probes were placed in central locations within each magnet with the largest field gradient. These probes were read out through a Gaussmeter display in the hut. These display units contained calibration offsets which were recorded for each magnet. All measurements are maintained on the gitHub repos: [11], [12], [4].

The general procedure was to ramp each magnet from 0 A to its maximum (approximate) current associated with 11 GeV running and then back to 0 A. Measurements were recorded in 10% increments when coming down from the maximum in order to ensure that measurements are on the hysteresis loop. Each measurement took approximately three minutes before the read out was considered reliable and stable (read out on the Gaussmeter display is unchanging). Measurements were taken at 0 A before and after changing the polarity. The magnet was then ramped to the same maximum current on the opposite polarity while recording the field values along the downward ramp of the hysteresis. The same field measurements were taken around 0 A while changing the polarity again. The third ramp was completed on the same polarity as the first ramp to provide a means of verifying repeatability of the field measurements.

In analysis of the offline data, the first check included the probe offsets from the Gaussmeter readout box. A general probe offset was calculated from the average difference between the 0 A current setting on both polarities. The data was then compared between the positive and negative polarities to determine a general uncertainty in the probe measurement. The assumption here is that the positive and negative polarities should yield the same measurement. This was later independently verified with using NMR probes (which do not have probe offsets), and the NMR probes yielded relative differences no larger than $1E-4$.

The measured points field points were then fit to a high order polynomial as a function of current. In this way, from a desired $\int Bdl$, one can precisely obtain the required set current. These polynomial fits were checked for their relative residual to validate the goodness of the fit at obtaining the current and to quantify the error on setting the magnet.

From a golden ratio of B_0/I_0 as determined from initial optics focusing and tuning, any changes to the linearity are applied from the function $\frac{B/I}{B_0/I_0}\frac{L_{eff,TOSCA}}{L_{eff,constant}}$. In all cases, only the **set current** is used (not the read back current). This is because the set current will always be the same to the power supply, but the read back current could change depending on various calibration parameters that are input to the power supply. Therefore, the read back current is somewhat irrelevant for analysis as the set current should be used when checking the magnet settings.

2.1. Horizontal Bender

The horizontal bender was studied with both $z-$dependent measurements along the length of the magnet as well as central measurements with the final side iron and installed front clamp configuration for the magnet. Original measurements of the effective length when compared to TOSCA (both without the final iron configuration) showed good agreement in Figs. 1 and 2 [11].

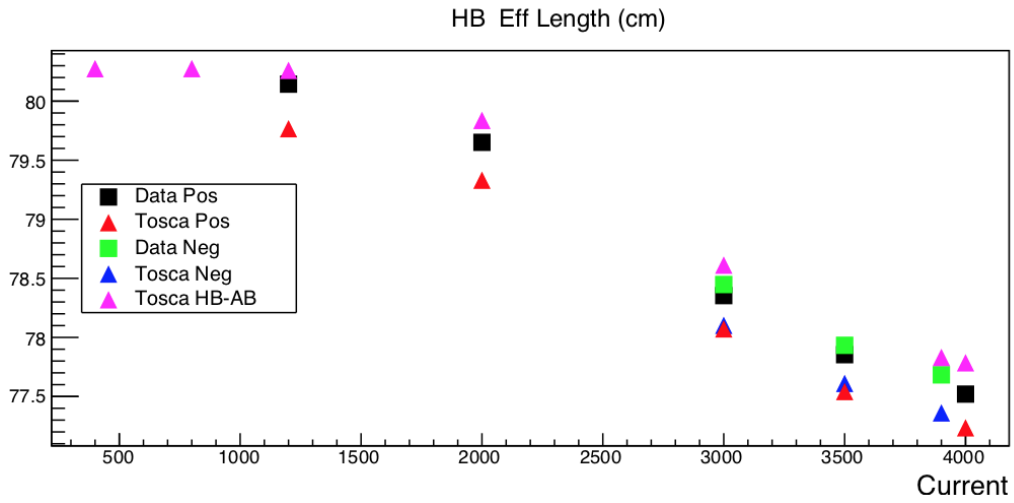

Figure 1: *Shown here is data (L_{eff}) from a positive and negative ramping of the HB prior to the installation of the final side iron and clamp. This data compares reasonably well with the corresponding TOSCA model.*

In Fig. 1, the TOSCA points show reasonable agreement with the data for the measured effective field length. The $\int Bdl$ comparison also agrees reasonably well and is shown in Fig. 2.

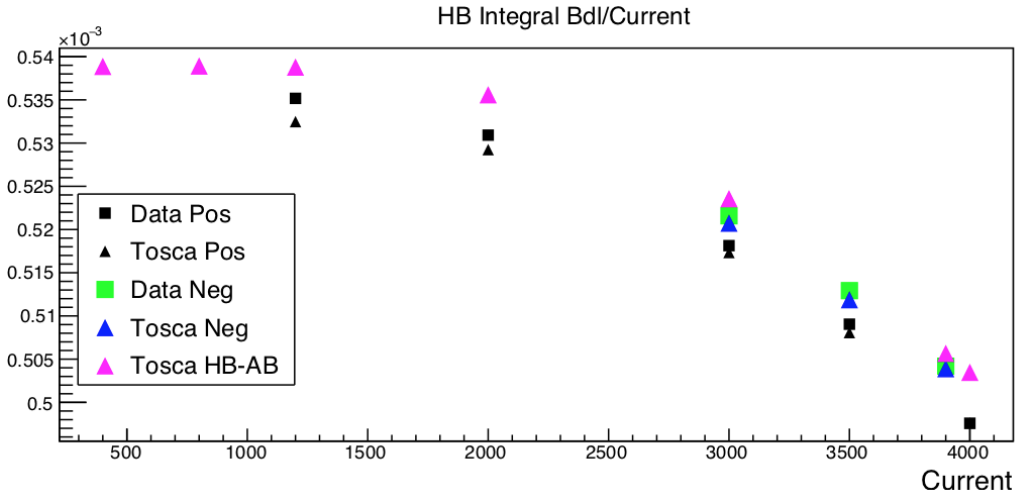

Figure 2: *Shown here is the data ($\int Bdl$) from a positive and negative ramping of the HB prior to the installation of the final side iron and clamp. This data compares reasonably well with the corresponding TOSCA model.*

The original TOSCA model (without final iron configuration) is compared with the v10 TOSCA model which was developed to model the final side iron and installed front clamp configuration that is used in current beam operations. The comparisons between these two models is shown in Fig. 3.

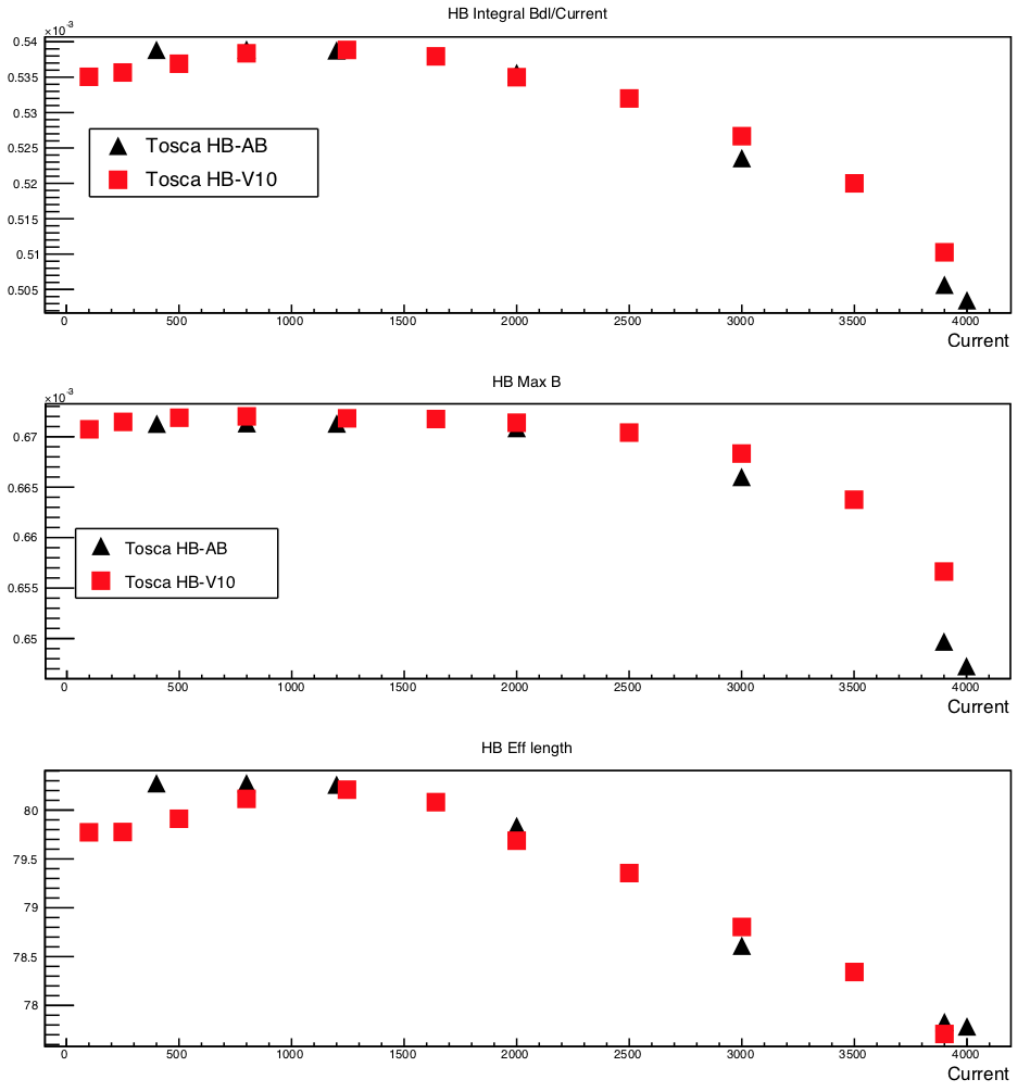

Figure 3: *The original TOSCA model without the side iron and clamp is described by the points in "TOSCA HB-AB." These points are directly compared to the TOSCA model with the modeled side iron and clamp as "TOSCA HB-V10." The points show discrepancies most significantly above 3000 A (approximately 8.5 GeV/c).*

The v10 TOSCA model shows a shallower drop off in the high momentum (current) tail at for the $\int Bdl$. z-dependent data measurements were never taken with the final side iron and installed front clamp configuration, but very detailed central field values were measured. These measurements were compared to anticipated values from TOSCA. These measurements were fit with a high order polynomial for the purposes of understanding the change in the $\frac{B/I}{B_0/I_0}$ curve. The polynomial fit relative residual is less than 0.02%. The probe errors in the measurement (by comparing the positive and negative polarity measurements with probe offsets accounted for) had a relative error no greater than 0.12%. The final central field ramp results are shown in Fig. 4.

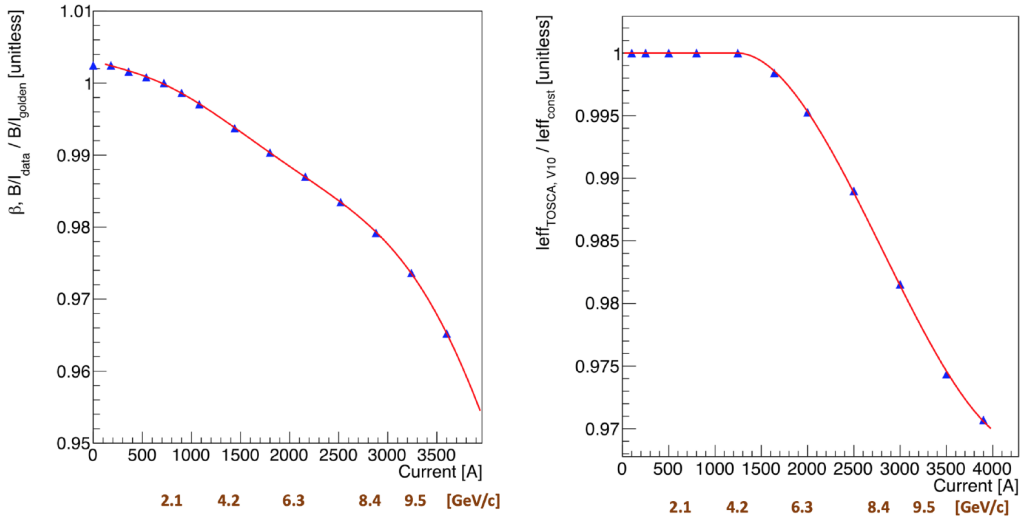

Figure 4: *On the left is shown the ratio of the measured B/I to a golden tune B_0/I_0 for the HB. The approximate corresponding momentum setting is shown below the x-axis. The ratio is set to 1 at the golden tune. On the right is shown the $L_{eff,TOSCA}/L_{eff,linear}$ to show the change in the effective field length as a function of current.*

On the left side of Fig. 4, the changing B/I curve relative to the golden tune B_0/I_0 is shown with a dramatic decrease as a function of current. The approximate momentum is shown below the x-axis. On the right side of Fig. 4, the L_{eff}/L_0 fit is shown for the latest TOSCA v10 model. This fit has a relative residual less than 0.028%. It is important to note that the measured values for setting the HB magnet in Fig. 4 differ from the saturation expected from TOSCA at high central momentum (more saturation than that in TOSCA). This discrepancy could arise from a difference of the probe position or a mis-modeling of the same probe position in TOSCA. Current beam data that could show if there is a problem in the setting of the HB goes through 8.5 GeV central momentum and does not presently indicate a problem in this range.

2.2. Q1

The SHMS Q1 was tested with various $z-$dependent measurements [12]. A central field measurement was completed over the summer of 2017. The data from this ramping is shown in Fig. 5. This data was consistent with previous data and had an overall probe relative error smaller than 0.2%.

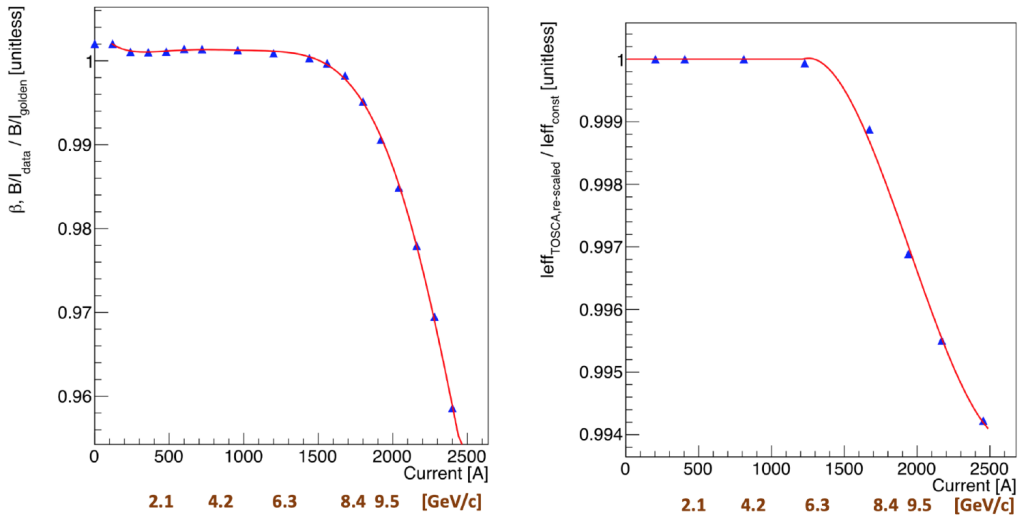

Figure 5: *On the left is shown the ratio of the measured B/I to a golden tune B_0/I_0 for Q1. The approximate corresponding momentum setting is shown below the x-axis. The ratio is set to 1 at the golden tune. On the right is shown the $L_{eff,TOSCA}/L_{eff,linear}$ to show the change in the effective field length as a function of current.*

On the left of Fig. 5 the data is fit with a high order polynomial having a relative residual of less than 0.06%. The drop off in the central field is consistent in shape with the TOSCA predictions (although somewhat less significant). The approximate corresponding central momentum is shown below the x-axis. The right plot shows the change in the effective field length. Several measurements in Q1 showed less saturation in B/I when compared to TOSCA at the same locations. To use the TOSCA effective field length, a small re-scaling correction was put in to lessen the saturation in the tails to better match the data. The scaling correction was applied as $1-(1-\frac{L_{eff,TOSCA}}{L_{eff,linear}})\frac{B_0-B_{data}}{B_0-B_{TOSCA}}$. This modifies the shape of $L_{eff,TOSCA}$ to be consistent with the measured values in data. The relative residual of the fit to the changing effective field length is less than 0.02%.

3 Setting the SHMS magnets

The SHMS magnets are set by current. A conservative cycling procedure of going to 300 A above the desired current before coming back down was established for running with beam. The cycling procedure is conservative and is recommended to be studied in more detail during a long down. The cycling procedure was developed by studying the repeatability of obtaining various field readbacks on the external probes during ramping. Only the Q1 magnet must always be ramped to a minimum of 1500 A with at least a 300 A buffer between the desired current and ramping current.

3.1. Field setting program

The program for setting the magnets is maintained at [1], and the various saturation models are contained in the code although many are commented out. The program finds the ideal current to

set each magnet at by iterating over the following ratio defined in Eq. (1).

$$\frac{P_i}{P_{desired}} = \frac{I_i}{I_{linear}} \frac{\beta(I_i)}{\beta_{golden}} \frac{L_{eff,i}}{L_{eff,golden}} \tag{1}$$

where the golden values are determined from the golden tune and β is defined to be B/I. The program takes the desired momentum as input. It then calculates a linear extrapolation from P/I to obtain an initial current, I_{iter}. This current is then iterated on until the correct value of the corresponding desired current is found for the desired momentum (i.e. the ratio $P_i/P_{desired}$ is within a defined tolerance).

3.2. Relevant changes to setting the magnets

The initial parameterizations for setting the magnets are designated in Version 0. Table 1 shows the factors assigned to Version 0 magnet setting. The final factors are shown in the column "P/I v6 factor" which includes the final factors applied to the P/I quantity when setting the magnets as contained in Version 6 of the magnet setting code. Some magnets included saturation models for B/I and/or L_{eff}, and the relevance to various versions is shown in the columns "B/I sat model?" and "L_{eff} sat model?". During the initial optics commissioning with one and three pass beam

Table 1: *Progression of the field setting model for data-taking.*

Magnet	B/I_{V0} **[kG/A]**	P/I_{V0} [kG/A]	B/I **sat model?**	L_{eff} **sat model?**	P/I **v6 factor**
HB	$6.485E-03$	0.003	v6	v6	0.983
Q1	$7.103E-03$	0.004	v0-v2, v6	v0-v2	0.983×0.97
Q2	$9.436E-03$	0.003	–	–	0.983×0.96
Q3	$9.728E-03$	0.004	v0-v2	–	0.983×0.97
dipole	$1.184E-02$	$3.188e-03$	v0-v5	–	0.983

in December of 2017, the quads were scaled by studying the sieve focal plane distributions in carbon elastic scattering. These initial changes produced Versions 1 and 2 of the field setting code. Saturation factors in HB, Q1, and Q3 are contained in Versions 0–2 of the setting code, but the saturations for Q1 and Q3 were found to be unnecessary in Version 3 of the code. Prior to the fall 2018 running, all magnets were updated with the approximate offset of 0.983 in Version 4, and the high momentum changes to the SHMS dipole were removed in Version 5. Version 6 was a modification to the Q1 magnet that fit a saturation effect seen in data between 6–8 GeV/c central momentum. The specific dates of the changes are listed below:

- **Version 1** Applied on December 11, 2017 at 4:21 am starting with SHMS run 1605. All quads are scaled by a factor of 1.05 times their nominal setting. The HB and dipole are not modified [5].
- **Version 2** Applied on December 19, 2017 at 9:06 am starting with SHMS run 1655. The original 1.05 scale factor for the quads is removed and modified to be: Q1 at 1.03, Q2 at 1.04, Q3 at 1.03 [6].
- **Version 3** Applied on April 5, 2018 at 3:47 pm starting with coincidence run 3288. The Q1 and Q3 saturation modifications (in the code) are completely removed [7].
- **Version 4 and 5** Applied on August 14, 2018 at 6:14 pm starting with SHMS run 4432, HMS run 2347, and coincidence run 4436. All SHMS magnets (HB, Q1, Q2, Q3, dipole) and scaled up

by a factor of 1/0.983 from the commissioning studies in order to better match the desired central momentum setting [8]. Additionally, any non-linear dipole modeling behavior is removed.

- **Version 6** Applied on September 29, 2018 at 5:06 pm starting with coincidence run 4780. A saturation model for Q1 is applied at 6 GeV and above: $1/(-0.00077P^2 + 0.0132P + 0.94938)$. This was not studied above 8.035 GeV central momentum and uses a constant value at and above 8.035 GeV from the equation.

4 Carbon elastic

During the initial commissioning with the SHMS at 7.5 degrees and at a central momentum of 2.214 GeV/c, the carbon target and sieve were used to identify carbon elastic events. The distribution and sieve pattern are shown in the data in Fig. 6.

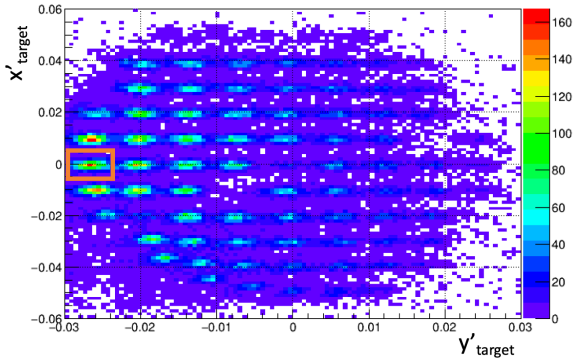

Figure 6: *Carbon sieve pattern using reconstructed target quantities at 2.214 GeV/c central momentum.*

The first order optics, as initially calculated from COSY, are shown in Fig. (**??**).

$$\begin{aligned} xfp(mm) &= -1.38 * xtar(mm) - 0.004 * xptar(mr) + 16.5 * delta \\ xpfp(mr) &= -.0602 * xtar(mm) - .72 * xptar(mr) + 3.2 * delta \\ yfp(mm) &= -1.6 * ytar(mm) - 0.03 * yptar(mr) - 1.5 * delta \\ ypfp(mr) &= -.268 * ytar(mm) - 0.61 * yptar(mr) + 0.074 * delta \end{aligned}$$

Figure 7: *First order optics as calculated from COSY.*

By selecting all the events from a single carbon sieve hole (outlined in orange in Fig. 6), the carbon energy spectrum can be calculated using the first order optics and known reconstructed quantities. This spectrum is shown in Fig. 8.

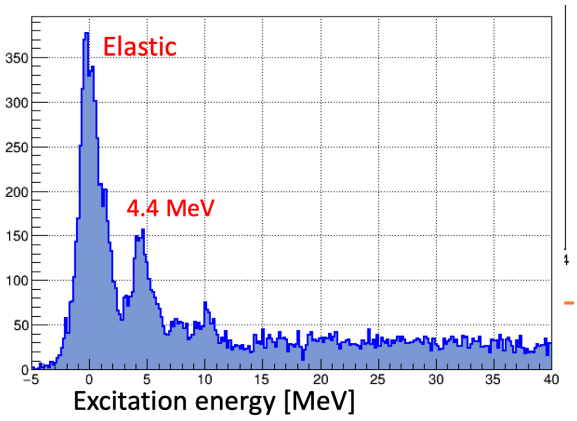

Figure 8: *The carbon elastic energy spectrum for events for a single sieve hole, as calculated in terms of delta from the first order optics, clearly shows the carbon elastic peak and the 4.4 MeV excited state.*

The carbon energy spectrum clearly shows the elastic peak and the 4.4 MeV carbon excited state. Additional carbon states are observable in the smaller peaks to the right of the 4.4 MeV peak.

5 Optimization of matrix elements

The general procedure for optimizing the SHMS matrix elements does not differ to the procedure used for the HMS matrix elements which is documented in detail at [2]. The code for optimizing the SHMS matrix elements is maintained in gitHub at [3]. The first matrix optimization for commissioning used runs taken with 3-pass beam energy at central momenta between 2 to 4 GeV/c and central angles from 15 to 30 degrees. This optimization was re-done in the winter of 2018 by eliminating the 4 GeV/c runs at 15 degrees and including a single foil run at 3 GeV/c and 9.5 degrees with a single foil. This was done to remove bias from the data taken with the mis-set Q1 and Q3 quads.

The general procedure is as follows: the events are initially reconstructed using the original reconstruction matrix elements. These events are used to determine the true physical values such as which foil an event originated from and which hole the event passed through in the sieve. The differences of the measured events with the real true physical values are minimized using Singular Value Decomposition (SVD) to calculate the optimized/improved reconstruction matrix elements.

5.1. Event Reconstruction

The event reconstruction calculates the target interaction point from the tracks reconstructed in the focal plane using the drift chambers. Target offsets, beam offsets and mis-pointings are important to account for when reconstructing events. The matrix elements consist of a set of coefficients followed by the value of the powers for each focal plane element. For example, a line in the reconstruction matrix elements is written in the following way:

$$X' \quad Y \quad Y' \quad D \quad ijklm \tag{2}$$

From Eq. (2), coefficients are X', Y, Y', and D, and the powers of each focal plane variable are represented by $ijklm$. The reconstruction equations are written as in Eq. (3).

$$
\begin{aligned}
x'_{tar} &= \sum_{ijklm} X'_{ijklm} x^i_{fp} x'^j_{fp} y^k_f p y'^l_{fp} x^m_{tar} \\
y_{tar} &= \sum_{ijklm} Y_{ijklm} x^i_{fp} x'^j_{fp} y^k_f p y'^l_{fp} x^m_{tar} \\
y'_{tar} &= \sum_{ijklm} Y'_{ijklm} x^i_{fp} x'^j_{fp} y^k_f p y'^l_{fp} x^m_{tar} \\
\delta_{tar} &= \sum_{ijklm} D_{ijklm} x^i_{fp} x'^j_{fp} y^k_f p y'^l_{fp} x^m_{tar}
\end{aligned} \tag{3}
$$

From Eq. (3), it is clear that the reconstruction is actually under-determined. For each event, we have four givens (x_{fp}, y_{fp}, x'_{fp}, y'_{fp}) and five unknowns to solve for (x_{tar}, y_{tar}, x'_{tar}, y'_{tar}, and δ). x_{tar} is never directly measured, but it is reconstructed with knowledge of the beam position and reconstructed values of y_{tar}, x'_{tar}, y'_{tar}. The x_{tar} independent terms are optimized from data while the x_{tar} dependent terms are from COSY. Attempts to fit these terms from data in 6 GeV era were unsuccessful, and COSY produced better values.

5.2. Focal plane

The focal plane distribution for the SHMS has been consistently offset to $+x_{fp}$. This was initially due to the tuning of the quads when the SHMS dipole was set approximately 1.7% low. Because the tuning was clearly observable using the 4.4 MeV excited carbon focal plane distributions, it was decided not to change the dipole relative to the quads and HB. As such, all magnets were scaled up by 1.7% starting August 2018. This will result in the x_{fp} always having an offset from zero. A recent distribution is shown in Fig. 9.

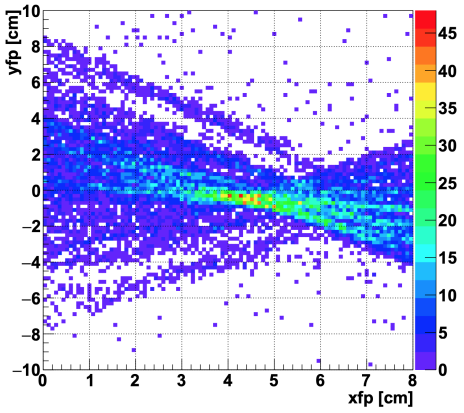

Figure 9: *The focal plane distribution is shown for run 6620. This run has a typical focal plane distribution that is shifted from $x_{fp} = 0$ due to the focusing of the SHMS quads when the SHMS dipole was originally offset by 1.7% central momentum.*

5.3. Optimization results

The matrix elements are used to reconstruct the interaction point of an event from the drift chamber tracks at the focal plane. The matrix optimization must include extended target optics so

that the reconstruction will be valid for the cryo target cells. The sieve is used for the optimization since each hole has an associated x'_{tar} and y'_{tar} that can be used for the optimization. The matrix elements that are optimized by using the code [3] are only the x'_{tar}, y'_{tar}, and y_{tar} terms. Separate studies were done to improve the optimization of δ. The runs relevant to the matrix optimization are shown in Fig. 10.

SHMS Matrix Optimization 2019						
Runs	Target	Pcentral	Theta	Sieve	Raster	Names
1813	optics 1	3.2*0.983	22.05	shifted	on	1813
1814	optics 1	3.2*0.983	22.05	centered	on	1814
1815, 1816, 1819, 1820, 1821, 1822	optics 2	2*0.983	30.065	centered	on	1815
1817, 1818, 1823	optics 1	2*0.983	30.065	centered	on	1817
coin: 1914, 1915, 1916, 1917, 1918	optics 1	2*0.983	30.075	centered	on	
coin 1919	optics 2	3.2*0.983	22	centered	on	1919
2233	optics 1	3.2*0.983	22	centered	on	
2234	optics 1	3.2*0.983	22	shifted	on	
2235, 2236, 2237, 2238, 2239	optics 1	2*0.983	30.02	centered	on	
6620	single foil	3.007	9.495	centered	off	6620

Figure 10: *The runs and conditions used for the optimization of the matrix elements are shown here. The colors correspond to runs that combined together due to similar angle, momentum, target, and sieve conditions. Runs shown in white are not combined with other settings.*

From the runs in Fig. 10, coincidence run 1919 was excluded from the fitting due to poor statistics. The runs at approximately 30 degrees also had poorer statistics, but they are necessary to include in order to extend the coverage of y_{tar}. The run at 6620 is useful, but should have included extended foils to improve the optimization. For runs grouped into the same kinematics as run 1814, the pre- and post-optimization sieve patterns are shown in Fig. 11.

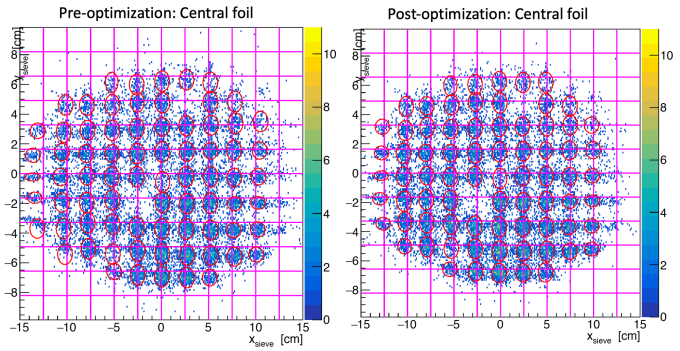

Figure 11: *The sieve pattern pre-optimizaiton is shown on the left and post-optimization is shown on the right. While there was a previous optimization performed in the early part of the commissioning, the latest results are not dramatic, but there are small improvements around the edges.*

In Fig. 11, the results are not significant as they were the first time an optimization was performed on the SHMS, but there does appear to be some improvement with the centering and around the edges. The effects of these changes are shown on the target reconstructed quantities in Fig. 12.

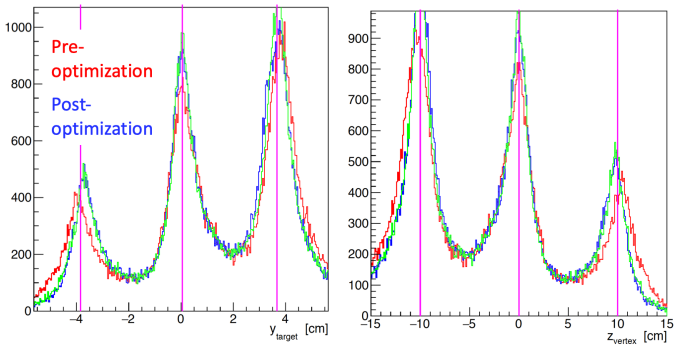

Figure 12: *The y_{tar} distribution is shown on the left for this particular run, and the corresponding z_{target} is shown on the right. The true value for the corresponding z_{target} is shown at the location of the magenta line. The red line is pre-optimization while the blue is post-optimization. A second optimization that excludes all runs at 30 degrees is shown in green, but this optimization does not work well for other extended target settings.*

From Fig. 12, the target quantities with the old matrix reconstruction elements are shown in red, and the new target quantities are shown in blue. There was a second comparable optimization that excluded the runs at 30 degrees (due to statistics) that is shown in green, but the results of this optimization are not ideal for all settings due to the lack of coverage in y_{tar} in the fit. This particular run has three foils and uses the centered sieve slit. The changes to the first order optics are small and are shown in Fig. 13.

First-order optics, pre-optimization

2.77714223e-01	-4.67264520e-02	3.03003269e-02	6.671533990e-01	10000
-1.4190911e+00	8.94882509e-02	-2.64692136e-02	-2.657067490e-01	01000
5.86545151e-03	-7.43039755e-01	3.13366030e-01	-1.280072910e-03	00100
-6.69934763e-02	1.32890907e+00	-2.00383133e+00	-8.94340584e-02	00010

First-order optics, post-optimization

2.773909307e-01	-5.227624519e-02	3.361287500e-02	6.671533990e-01	10000
-1.408758385e+00	8.945881400e-02	-3.358497180e-02	-2.657067490e-01	01000
1.021502672e-02	-7.810829752e-01	3.286485087e-01	-1.280072910e-03	00100
-8.585053002e-02	1.588583025e+00	-2.096608135e+00	-8.943405840e-02	00010

Figure 13: *The first order optics are shown for both the pre-optimization and post-optimization. The changes to the overall first order optics are small.*

The new first order optics are shown in Fig. 13, and the values can be compared to the previous first order optics. The changes to the coefficients are generally small indicating that the new optimized fit is not so different from the previous one. The corresponding x'_{tar} offset from the 0000 order matrix elements is -8.093640059e-04. These new matrix elements are in the usual hallc_replay DATFILES directory as “shms-2019-newopt-Jan19.dat."

5.4. Mis-pointings from surveys

The mis-pointing surveys are explained in detail here: [10]. Included below are the relevant mis-pointing parameterizations for the SHMS data as used in the matrix optimization.

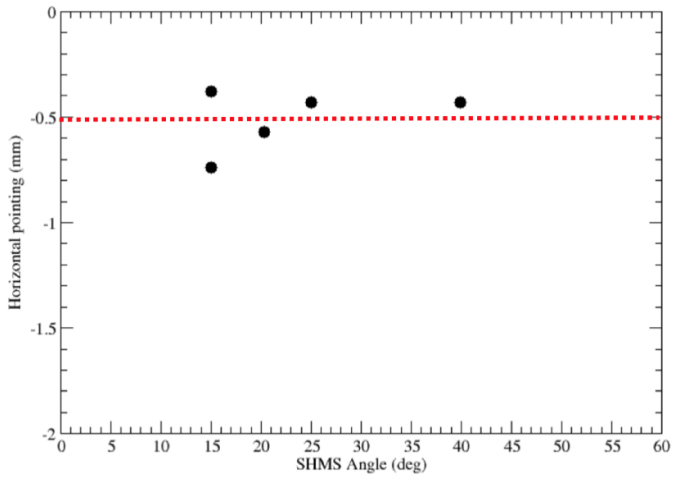

Figure 14: *The horizontal mis-pointing data is shown from survey. The red line indicates the constant value used for the mis-pointing with a value of $y_{mp} = -0.5mm$ [10].*

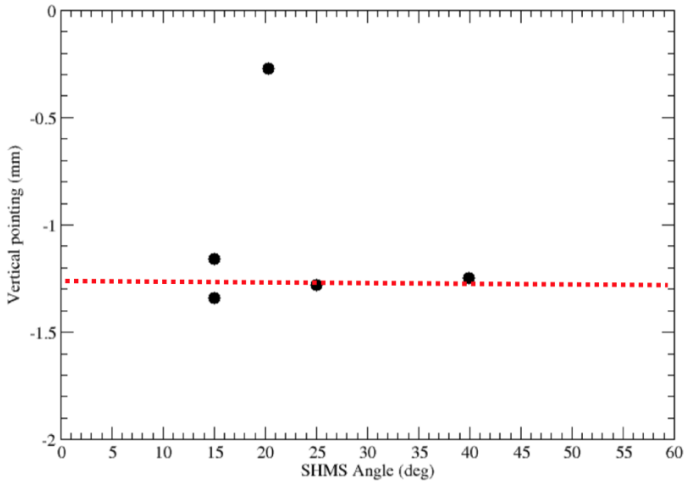

Figure 15: *The vertical mis-pointing data is shown from survey. The red line indicates the constant value used for the mis-pointing with a value of $x_{MP} = -1.26mm$ [10].*

The mis-pointing data has several inconsistent measurements for various angles. With further time and resources, it would be interesting to re-take some of this data to try to reconcile the differences.

6 Conclusion

This note records the measurements and setting parameters for the SHMS magnets beginning with the commissioning runs in Hall C. The overall performance of the SHMS is still being studied in detail through ongoing experiments, but the preliminary analysis shows performance to be within expectation. At this point, only the HB and Q1 magnets include a saturation effect in the

setting of the magnets. The performance at higher momentum above 8.5 GeV has not yet been rigorously evaluated with beam. An improvement in the statistics of various optics target runs at various y_{tar} settings is recommended and would improve the matrix optimization results.

7 Appendix

7.1. Maps

Here I mention the coincidence map files as these runs span a long range in time, and the maps used in replay must be modified, accordingly. For all runs in 2017–spring 2018, the map should be "coin_comm18.map." For maps in the fall 2018, the appropriate map is "coin.map."

7.2. Beam position and raster information

For doing the matrix optimization correctly, it is essential to use the correct fast raster and beam position monitor (BPM) calibrations and offsets. These parameters are contained in HallC Replay in gbeam.param. The following constants were verified and used for the replay and optimization of the SHMS matrix elements.

Winter 2017 BPM Parameters: gbpmxa_slope = -0.98 gbpmxa_off = -0.05 gbpmxb_slope = -1.12 gbpmxb_off = +0.08 gbpmxc_slope = -0.96 gbpmxc_off = -0.89 gbpmya_slope = 0.97 gbpmya_off = -0.20 gbpmyb_slope = 1.17 gbpmyb_off = 0.38 gbpmyc_slope = 0.87 gbpmyc_off = 0.47 **;positions of BPMs relative to target (from Fall 2017 survey)** gbpma_zpos = 320.42 ; cm gbpmb_zpos = 224.86 ; cm gbpmc_zpos = 129.44 ; cm	**;Raster constants determined for Winter 2017 run 1565** gfr_cal_mom = 2.218 gfrxa_adc_zero_offset = 65200 gfrxb_adc_zero_offset = 67050 gfrya_adc_zero_offset = 67200 gfryb_adc_zero_offset = 65650 gfrxa_adcpercm = 67000.0 gfrxb_adcpercm = 62666.6 gfrya_adcpercm = 56333.3 gfryb_adcpercm = 56000 **;positions of FR magnets relative to target** gfrx_dist = 1375 ; cm gfry_dist = 1337 ; cm

Figure 16: *The BPM and raster values that should be used in gbeam.param to replay runs in December 2017.*

Spring 2018 BPM Parameters:
gbpmxa_slope = -0.98
gbpmxa_off = -0.05
gbpmxb_slope = -1.12
gbpmxb_off = +0.08
gbpmxc_slope = -0.96
gbpmxc_off = -0.89
gbpmya_slope = 0.97
gbpmya_off = -0.20
gbpmyb_slope = 1.17
gbpmyb_off = 0.38
gbpmyc_slope = 0.87
gbpmyc_off = 0.47
;positions of BPMs relative to target (from Fall 2017 survey)
gbpma_zpos = 320.42 ; cm
gbpmb_zpos = 224.86 ; cm
gbpmc_zpos = 129.44 ; cm
	;Raster constants determined for Jan 2018 3 pass
	gfr_cal_mom = 6.4
	gfrxa_adc_zero_offset = (75733.+51938.)/2.;
	gfrxb_adc_zero_offset = (79778.+57293.)/2.;
	gfrya_adc_zero_offset = (77755.+57411.)/2.;
	gfryb_adc_zero_offset = (71093.+52056.)/2.;
	gfrxa_adcpercm = (75733.-51938.)/0.2;
	gfrxb_adcpercm = (79778.-57293.)/0.2;
	gfrya_adcpercm = (77755.-57411.)/0.2;
	gfryb_adcpercm = (71093.-52056.)/0.2;
	
	;positions of FR magnets relative to target
	gfrx_dist = 1375 ; cm
	gfry_dist = 1337 ; cm

Figure 17: *The BPM and raster values that should be used in gbeam.param to replay runs in January through May 2018.*

Fall 2018 BPM Parameters: gbpmxa_slope = -0.98 gbpmxa_off = -0.05+0.21 gbpmxb_slope = -1.12 gbpmxb_off = +0.08+0.12 gbpmxc_slope = -0.96 gbpmxc_off = -0.89-0.29 gbpmya_slope = 0.97 gbpmya_off = -0.20+0.36 gbpmyb_slope = 1.17 gbpmyb_off = 0.38+0.36 gbpmyc_slope = 0.87 gbpmyc_off = 0.47+0.31 **;positions of BPMs relative to target (from Fall 2018 survey)** gbpma_zpos = 320.17 ; cm gbpmb_zpos = 224.81 ; cm gbpmc_zpos = 129.38 ; cm	**;Raster constants determined from coin run 4556 on Aug 20, 2018** gfr_cal_mom = 8.518 gfrxa_adc_zero_offset = 64150 gfrxb_adc_zero_offset = 66250 gfrya_adc_zero_offset = 67700 gfryb_adc_zero_offset = 64100 gfrxa_adcpercm = 158000 gfrxb_adcpercm = 147000 gfrya_adcpercm = 155500 gfryb_adcpercm = 157500 **;positions of FR magnets relative to target** gfrx_dist = 1375 ; cm gfry_dist = 1337 ; cm

Figure 18: *The BPM and raster values that should be used in gbeam.param to replay runs in August through December 2018.*

7.3. Magnet modeling not validated by data

Included below is the erroneous model for the Q3 saturation that was applied to the running between January to April 2018.

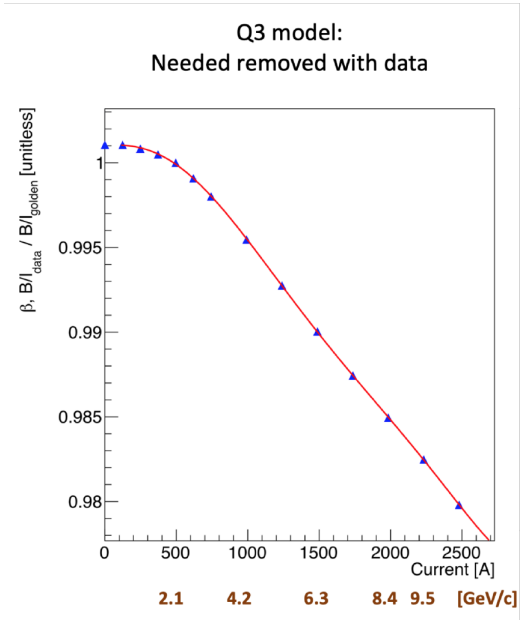

Figure 19: *Q3 β/β_{golden} as measured during the summer of 2018. This model is not supported by TOSCA and was removed in April 2018.*

Additionally, shown below is the NMR measured dipole central field response. These results were precise and repeatable and should be explored at high central momentum.

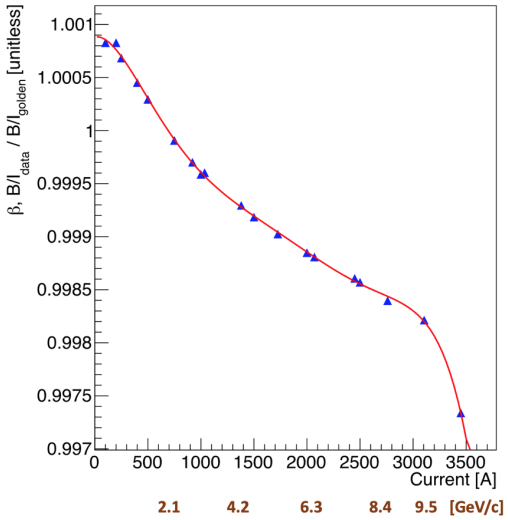

Figure 20: *Spectrometer dipole β/β_{golden} as measured during the summer of 2018 using NMR probes. This model is not supported by TOSCA and was removed in August 2018.*

References

[1] field17 gitHub repository, https://github.com/JeffersonLab/field17

[2] Bericic, J., Notes on the HMS Optics, https://hallcweb.jlab.org/DocDB/0008/000849/001/HMS_optics_notes.pdf

[3] SHMS optics matrix optimization gitHub repository, https://github.com/hszumila/SHMS_optics

[4] Magnetic field studies of the SHMS magnets and HMS dipole, https://github.com/hszumila/magnets

[5] https://logbooks.jlab.org/entry/3502390

[6] https://logbooks.jlab.org/entry/3506891

[7] https://logbooks.jlab.org/entry/3555447

[8] https://logbooks.jlab.org/entry/3587052

[9] magnet testing gitHub repo, https://github.com/hszumila/magnets

[10] Mis-pointing survey summary, https://github.com/MarkKJones/fall2017-plans/blob/master/Surveys/survey-summary.pdf

[11] HB mapping data in repository, https://github.com/MarkKJones/hb-mapping-data

[12] Q1 mapping data in repository, https://github.com/MarkKJones/q1-mapping-data